

# REAL-TIME IMPLEMENTATION OF ESOGI-FLL-BASED SPEED-SENSORLESS CONTROL FOR INDUCTION MOTOR DRIVES WITHIN ELECTRIC VEHICLE SYSTEMS

MOHAMMED BOUKHARI<sup>1</sup>, RIAD BOUZIDI<sup>2</sup>, ISMAIL GHADBANE<sup>3</sup>,  
BELHOUCHE KHALED<sup>4</sup>, AHMED BENDIB<sup>5</sup>, KHERBACHI ABDELHAMMID<sup>6</sup>

## Abstract

This paper proposes an enhanced method for estimating the speed of a three-phase induction motor (IM) using an improved second-order generalized integrator-based frequency-locked loop (ESOGI-FLL) designed explicitly for effective DC offset rejection. The proposed ESOGI-FLL-based speed estimation technique is seamlessly integrated into a sensorless control scheme, improving the overall control performance of the IM under various operating conditions, including scenarios with significant DC disturbances. The method ensures a smoother and more stable speed estimation by accurately determining the motor's operating frequency and effectively suppressing ripples caused by DC offset. A key advantage of this approach is its reliance on a single current sensor, which simplifies implementation and enhances the system's robustness against external noise and disturbances. Extensive experimental results validate the efficacy of the proposed technique, demonstrating reliable and accurate performance over a broad speed range.

<sup>1</sup> Department of Electrical Engineering, Electrical Engineering Laboratory, M'sila University, M'sila, Algeria, e-mail: mohammed.boukhari@univ-msila.dz, ORCID: 0000-0001-5770-3020

<sup>2</sup> Department of Electrical Engineering, Electrical Engineering Laboratory, M'sila University, M'sila, Algeria, e-mail: riad.bouzidi@univ-msila.dz, ORCID: 0000-0002-3440-8624

<sup>3</sup> Department of Electrical Engineering, Electrical Engineering Laboratory, M'sila University, M'sila, Algeria, e-mail: ismail.ghadbane@univ-msila.dz, ORCID: 0000-0003-1860-0699

<sup>4</sup> Department of Electrical Engineering, Electrical Engineering Laboratory, M'sila University, M'sila, Algeria, e-mail: khaled.belhouchet@univ-msila.dz, ORCID: 0009-0008-0963-441X

<sup>5</sup> Department of Electrical Engineering, Electrical Engineering Laboratory, M'sila University, M'sila, Algeria, e-mail: ahmed.bendib@at.dz, ORCID: 0000-0002-7689-8692

<sup>6</sup> Renewable Energy Development Center, Algiers, Algeria, e-mail: a.kherbachi@cder.dz, ORCID: 0000-0002-6166-7744

The method's robustness and simplicity make it a promising solution for high-performance sensorless control of IMs in industrial applications.

**Keywords:** enhanced second-order generalized integrator-frequency locked loop (ESOGI-FLL); induction motor (IM); speed estimation; sensorless control; DC disturbance; electric vehicle (EV)

## 1. Introduction

The evolution of industrial systems towards automated processes requires integrating and controlling electric motors in an electronic regulation environment. Accordingly, the DC motor, whose electric model suggests simple control laws, occupies a large share of the electric motors [1]. However, this machine's main physical weaknesses are linked to a mechanical commutator's presence. To this end, the research has been oriented toward other types of motors. Permanent magnet synchronous motor (PMSM) offers high efficiency and power density due to permanent magnets on the rotor, providing precise control and excellent performance at high speeds. However, it is expensive because of the rare earth materials used in magnets [2]. Brushless DC motors (BLDC) combine the advantages of PMSM and DC motors with high efficiency, compact size, and reduced maintenance since they lack brushes. Unfortunately, their torque ripple still can be a significant limitation [3]. Switched reluctance motors (SRM) are low-cost, simple, and highly robust, with excellent fault tolerance. Still, they produce more noise and vibration, and their control systems are complex due to nonlinear torque characteristics [4]. Lastly, induction motors (IM) are robust, reliable, cost-effective, and widely used in industrial and EV applications [5]. In IM drives, mechanical speed sensors have been widely used for speed sensing. Although these sensors can deliver precise speed data across a broad range, they have drawbacks such as decreased dependability and higher cost [6]. Therefore, the speed-sensorless control strategy based on speed estimation has experienced significant development. However, estimation methods' simplicity, accuracy, and robustness to disturbances are challenging tasks that ensure the control of IMs with high performance.

Numerous research studies concerning estimation-based-sensorless control of motor speed have recently been proposed [7]. In these researches, different techniques have been used to estimate the IM speed, such as an adaptive reference model system (ARMS), which has some drawbacks, including sensitivity to incorrect reference models and the precision of the ARMS estimator is heavily influenced by the quality of the used reference model. More particularly, if the reference model is not adequately suited to the actual system, the estimator's performance may be poor and can be sensitive to disturbances and noise present in the system, which may lead to inaccurate estimation [8]. The extended Kalman filter has been proposed for IM speed estimation. Although the EKF is a powerful method in nonlinear systems, it has some limitations and drawbacks that must be considered. A good

understanding of the underlying system is required to specify the process and observation models [9] correctly. An artificial neural network (ANN) observer has been adopted in [8], which has offered advantages such as the ability to model complex nonlinear systems. Still, it also has disadvantages related to its design, data requirements, and interpretability [8]. These factors should be considered when evaluating their suitability for a given application. Observers for speed sensorless IM drives exhibit increased complexity and nonlinearity. As a result, these approaches are unsuitable for industrial use at this stage [10–12]. In addition, all the closed-loop above estimation techniques rely on stator motor side current and voltage measurements, which could subject the speed calculation to measurement noise. Furthermore, generally speaking, the methods mentioned above require costly voltage and current sensors, at least two sensors, and most lack filtering algorithms to enhance speed estimation [13].

To bridge this gap, an effective solution for speed estimation (or flux estimation), the SOGI-FLL method, has been suggested in [14–16], and it has successfully relied on the drive system's recommended control strategy. The findings of [16] have shown that the suggested technique has improved the speed estimation accuracy, its simplicity of implementation, and the use of only one current sensor, reducing the system cost. However, the major drawback of the SOGI-FLL-based estimation is the presence of the DC offset in its input current, which may affect the accuracy of frequency estimation. More particularly, it may result in undesirable ripples in the estimated frequency and a shifted quadrature component, hence, may threaten the system stability.

To overcome this issue, an innovative speed estimation method based on an ESOGI-FLL method suitable for the rejection of the DC offset is proposed in this paper. The ESOGI-FLL has the same performance as the SOGI-FLL in terms of ease of implementation, rapid transient response, and harmonic rejection capability, in addition to its ability to eliminate the effect of the DC disturbance. All this can ensure an accurate estimation of the IM operating speed, even in the presence of severely distorted current. Furthermore, the system cost can be reduced due to the need for only one current sensor, a single loop, to design the IM motor control. The implementation of the proposed control strategy in the dSPACE Micro LabBox platform is conducted to assess its effectiveness. The results showed that the designed control scheme ensures an accurate angle speed estimation and is more effective when driving the IM under disturbances.

The rest of this paper is arranged as follows: Section 2 describes the proposed control scheme. Section 3 discusses the stability of the used method. Section 4 deals with the experimental setup and discusses the results. Section 5 summarizes the paper's findings.

## 2. Control of the IM drive system

The structure of the IM motor system controlled by the proposed scheme is depicted in Figure 1. As seen, the IM is derived based on an inverter, which feeds by a DC source and its switches controlled by a PWM. The control scheme consists of a DTC controller and an ESOGI-FLL to estimate the operating frequency from the measured current. The frequency estimate is used to detect the angular speed and then sent to the DTC control block to be adjusted to its speed reference using a PI controller. A Hysteresis control unit handles the resulting signal to generate the PWM duty cycle. More details of the proposed scheme will be provided in the following section.

The regulation of the IM speed can be achieved by manipulating the voltage and frequency of the stator to desired references. The goal is maintaining the air gap flux at a consistent, designated value during steady-state conditions. This method is called scalar control because it concentrates on the steady state. Consequently, the equation demonstrates the direct impact of the electric frequency  $\omega_s$  and the stator's phase voltage ratio on the stator flux [17]:

$$V_s = R_s i_s + j\omega_s \phi_s \quad (1)$$

At high speeds, the term  $R_s$  becomes negligible compared to  $\omega_s$ , and to ensure that the stator flux ( $\phi_s$ ) remains constant across a range of speeds, the ratio of  $V_s$  to  $f_s$  must be consistently maintained. The frequency and the amplitude of the stator voltage have an equation that can be expressed as follows:

$$\frac{V_s}{f_s} = 2\pi\phi_s = \text{Const} \quad (2)$$

When the stator flux is held constant, the slip speed determines the electromagnetic torque, resulting in an almost linear relationship between torque and slip. To keep the flux's ( $\phi_s$ ) value constant, the ratio of  $V_s/f_s$  must remain constant throughout all speeds. Therefore, the stator voltages must also increase proportionately to maintain a consistent ratio of  $V_s/f_s$  as the speed rises. With no load, the slip is negligible, causing the rotor speed ( $\omega_r$ ) to match the synchronous speed ( $\omega_s$ ) closely. Due to this, open-loop scalar control fails to regulate speed effectively. Speaking of which, a closed-loop controller with speed-measuring capabilities is needed for applications that require high-speed precision and better responses to variations in the reference speed or the resistance torque. The following equation describes the mechanical dynamics of the induction motor:

$$\Omega_r = (T_{em} - T_r) - \frac{1}{Js + K_f} \quad (3)$$

$K_f$  is the viscosity coefficient,  $T_{em}$  represents the electromagnetic torque,  $\Omega_r$  is the rotor mechanical speed on rpm,  $T_r$  is the resistance torque, representing the load applied to the motor,  $J$  is the moment of inertia and  $s$  presents the Laplace operator.

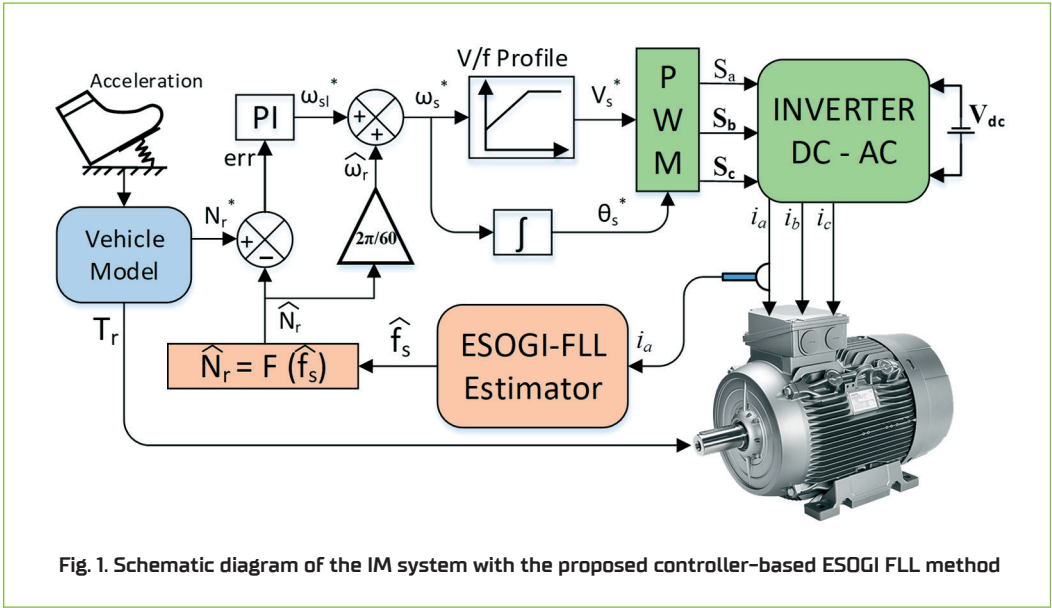


Fig. 1. Schematic diagram of the IM system with the proposed controller-based ESOGI FLL method

### 3. Proposed control scheme based on ESOGI-FLL

Figure 1 shows the structure of the proposed control scheme. This scheme includes the ESOGI FLL technique, which is employed to estimate the frequency accurately. ( $\hat{f}_s$ ) from a single-phase stator current that is detected by a single sensor. Consequently, the motor's estimated rotor speed ( $\hat{N}_r$ ) is determined by the function  $F$ , which is described in [4] below. After that, a PI controller examines the error to get the slip speed reference.  $\omega_{sl}^*$ . The restriction on this slip speed is for stability and overcurrent protection. Next, the synchronous speed reference,  $\omega_s^*$  is obtained by adding  $\omega_{sl}^*$  to  $\hat{\omega}_r$ . Consequently, the angular phase reference  $\theta_s^*$  is achieved by using the scalar control technique, while the voltage amplitude reference  $V_i^*$  is derived by integrating  $\omega_s^*$ . The inverter's signal commands ( $S_i$ ) are produced using these references,  $V_i^*$  and  $\theta_s^*$ , through a pulse width modulator [PWM].

$$\hat{N}_r = \frac{60\hat{f}_s}{p}(1 - S) \tag{4}$$

According to Figure 1, the mathematical formula of the actual rotor speed regulation to its estimate, which provides the slip speed reference,  $\omega_{sl}^*$ , can be derived as follows:

$$\omega_{sl}^* = k_p(N_r^* - \hat{N}_r) + k_i \int (N_r^* - \hat{N}_r) \tag{5}$$

where  $k_p$  and  $k_i$  are the PI controller's proportional and integral gains.

### 3.1. ESOGI-FLL technique

#### a. Structure of the ESOGI-FLL and modeling

The ESOGI-FLL technique is an adaptive filter that can reject DC disturbances, enabling accurate estimation of essential parameters associated with a single-phase sinusoidal signal, orthogonal components, amplitude, frequency, and phase angle. Figure 2 displays the ESOGI-FLL architecture, where  $v$  represents the input voltage,  $v_{\alpha}$  and  $v_{\beta}$  are the in-phase and quadrature-phase voltage estimates, and  $\hat{\omega}$  is the estimated frequency [18, 19]. This structure consists of two blocks: ESOGI and FLL. The ESOGI, which is a SOGI-based filter scheme, is composed of (i) adaptive second-order band-pass filters for the direct and quadrature voltages ( $\hat{v}_{\alpha}$  and  $\hat{v}_{\beta}$ ), tuned at the center frequency ( $\hat{\omega}$ ) provided by the FLL block, and (ii) To estimate the DC component from an input signal, LPF is incorporated into the common SOGI-FLL. The estimated DC component is rejected from the quadrature component voltage and the calculated error ( $e$ ) between  $v_i$  and  $\hat{v}_{\alpha}$  voltages. Incorporating this notion enhances the immunity of the SOGI-FLL against the disturbance effect caused by the direct current (DC) component, hence augmenting its filtering capacity for sub-harmonics. The mathematical expressions of the outputs of the ESOGI  $\hat{v}_{\alpha}$  and  $\hat{v}_{\beta}$  are given in the  $s$ -domain as follows [18]:

$$\hat{v}_{\alpha}(s) = \frac{k\hat{\omega}s}{s^2 + k\hat{\omega}s + \hat{\omega}^2} \cdot v_i(s) \quad (6)$$

$$\hat{v}_{\beta}(s) = \frac{k(\hat{\omega}^2 - \omega_f s)}{s + \omega_f} \frac{s}{s^2 + k\hat{\omega}s + \hat{\omega}^2} \cdot v_i(s) \quad (7)$$

Being  $\omega_f$  the cut-off frequency of the LPF is the gain of the ESOGI chosen as a trade-off between the speed of dynamic response and filtering capability. The FLL block is in charge of estimating the operating frequency of a sinusoidal input voltage. According to Figure 2, the estimated frequency by the ESOGI-FLL can be expressed as:

$$\hat{\omega} = -\frac{\gamma}{s} (v_i(s) - \hat{v}_{\alpha}(s) - v_{DC}(s)) \cdot \hat{v}_{\beta}(s) \quad (8)$$

where the FLL gains  $\gamma$  which has the following definition:

$$\gamma = \frac{k\hat{\omega}}{V^2} \Gamma \quad (9)$$

The estimated amplitude is represented by  $V$ , and  $\Gamma$  presents a positive gain of the FLL.

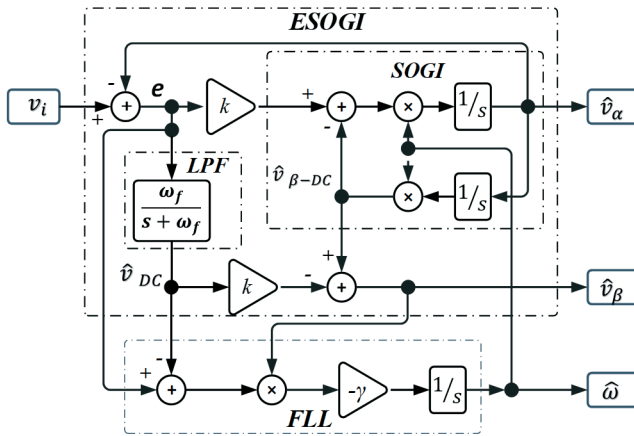


Fig. 2. The structure of the proposed control system

**b. Accuracy Assessment**

A test evaluates the ESOGI-FLL's performance in the Matlab/Simulink environment. In this test, an unexpected frequency fluctuation from 50 Hz to 52 Hz is analyzed in the ESOGI-FL; also, a distorted voltage with a significant DC component of 0.1 p.u. and low-order harmonics are considered. The magnitude of harmonics is  $V3=0.045$  p.u,  $V7=0.02$  p.u,  $V5=0.03$  p.u. Table 1 provides a summary of the ESOGI-FLL's parameters.

Tab. 1. ESOGI-FLL parameters

Parameters	Symbol	Unit	Value
ESOGI gain	$k$	-	0.85
FLL gain	$\Gamma$	s-1	50
LPF cut-off frequency	$\omega_f / 2\pi$	Hz	28

The ESOGI-FLL responses are displayed in Figure 3(a) and (b). The input voltage charts are shown in Figure 3(a).  $v_i$ , and the output orthogonal voltages,  $\hat{v}_\alpha$  and  $\hat{v}_\beta$ . Figure 3(b) shows the transient response of the frequency estimate. Figure 3(a) indicates that the ESOGI-FLL provides high harmonic filtering capability and DC component rejection. Figure 3(b) demonstrates that a precise determination of the operational frequency with a high speed of response is achieved. Consequently, the ESOGI-FLL is very useful for accurately estimating a motor's angular frequency [angular speed], even when the current is distorted.

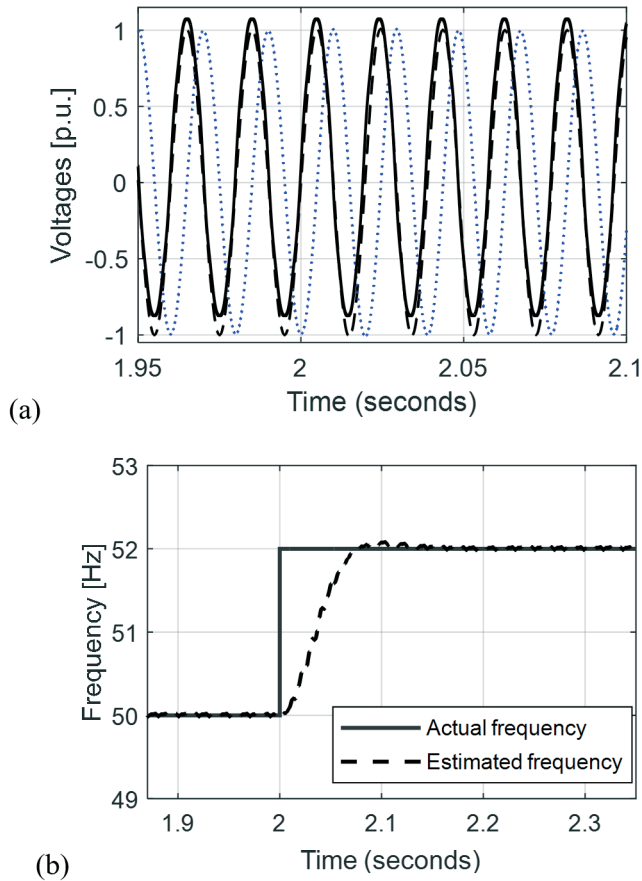


**Fig. 3. Obtained ESOGI-FLL results in response to frequency step perturbation of 2 Hz: [a] input and output voltages and [b] actual and estimated frequency**

### c. Stability evaluation of the ESOGI-FLL method

As stated in [20], stability is assessed using the nonlinear Lyapunov method to confirm the convergence of the proposed method. By considering the transfer functions, which correspond respectively to  $v_\alpha$ ,  $v_\beta$ , and the DC offset output of the LPF filter, we can derive the equations for the state space as follows:

$$\dot{x} = \begin{bmatrix} \dot{x}_1 \\ \dot{x}_2 \\ \dot{x}_3 \end{bmatrix} = Ax + Bv = \begin{bmatrix} 0 & 1 & 0 \\ -\hat{\omega}^2 & -k\hat{\omega} & 0 \\ 0 & -\omega_f & -\omega_f \end{bmatrix} \begin{bmatrix} x_1 \\ x_2 \\ x_3 \end{bmatrix} + \begin{bmatrix} 0 \\ k\hat{\omega} \\ \omega_f \end{bmatrix} [v] \quad (10)$$

$$y = \begin{bmatrix} v_\alpha \\ v_{\beta-DC} \\ v_{DC} \end{bmatrix} = Cx = \begin{bmatrix} 0 & 1 & 0 \\ \hat{\omega} & 0 & 0 \\ 0 & 0 & 1 \end{bmatrix} \begin{bmatrix} x_1 \\ x_2 \\ x_3 \end{bmatrix} \quad (11)$$

$$\dot{\hat{\omega}} = -\gamma(\hat{\omega}x_1 - kx_3)(v - x_2 - x_3) \tag{12}$$

In this expression, the variables  $y$  and  $x$  represent the output vectors and the state, while " $\dot{x}$ " denotes the first-order derivative of the proposed frequency. When the input voltage comprises the AC and the DC of the current components, a superposition method is employed to analyze the output vector in steady-state; thus, for an input voltage composed of  $v = v_{DC} + v_{AC}$ , the state vector ' $x$ ' and output vector ' $y$ ' are defined as follows:

$$\begin{cases} x = x_{DC} + x_{AC} \\ y = y_{DC} + y_{AC} \end{cases} \tag{13}$$

where  $v_{DC/AC}$ ,  $x_{DC/AC}$ , and  $y_{DC/AC}$  are the input voltage, the state vector contains the direct current components [DC], while the output vector consists of the AC components. By inserting (13) into (10) and (11), the following state-space equations in the steady state can be obtained.

• **In the scenario of a continuous analysis:** ( $v_{AC}=0, v_{DC}=V_{DC}$ )

$$\dot{\bar{x}}_{DC} = \begin{bmatrix} \dot{\bar{x}}_{1-DC} \\ \dot{\bar{x}}_{2-DC} \\ \dot{\bar{x}}_{3-DC} \end{bmatrix} = \begin{bmatrix} 0 \\ 0 \\ 0 \end{bmatrix} \tag{14}$$

$$\bar{x}_{DC} = \begin{bmatrix} \bar{x}_{1-DC} \\ \bar{x}_{2-DC} \\ \bar{x}_{3-DC} \end{bmatrix} = \begin{bmatrix} \frac{k}{\hat{\omega}} V_{DC} \\ 0 \\ V_{DC} \end{bmatrix} \tag{15}$$

$$\bar{y}_{DC} = \begin{bmatrix} \bar{v}_{\alpha-DC} \\ \bar{v}_{\beta-DC-DC} \\ \bar{v}_{DC-DC} \end{bmatrix} = \begin{bmatrix} 0 \\ kV_{DC} \\ V_{DC} \end{bmatrix} \tag{16}$$

In the case of DC analysis, where  $V_{DC}$  indicates the input voltage's DC component. For the alternative analysis, when  $v_{AC}=V_{Max} \sin(\omega t+\phi)$  and  $v_{DC}=0$ , and turning off the loop that estimates frequency ( $\hat{\omega} = 0$ ) the following scenarios are proposed.

When the system operates stably ( $\hat{\omega} = \omega$ ), the status and output vectors can be determined. The variables  $v_{DC/AC}$ ,  $x_{DC/AC}$  and  $y_{DC/AC}$  define the output and state vectors while distinguishing between the direct and alternating components of the input voltage.

The following steady-state equations can be determined by substituting (13) into (14)–(16).

$$\dot{\bar{x}}_{AC} = \begin{bmatrix} \dot{\bar{x}}_{1-AC} \\ \dot{\bar{x}}_{2-AC} \\ \dot{\bar{x}}_{3-AC} \end{bmatrix} = \begin{bmatrix} 0 & 1 & 0 \\ -\omega^2 & 0 & 0 \\ 0 & 0 & 0 \end{bmatrix} \begin{bmatrix} \bar{x}_{1-AC} \\ \bar{x}_{2-AC} \\ \bar{x}_{3-AC} \end{bmatrix} \tag{17}$$

$$\bar{x}_{AC} = \begin{bmatrix} \bar{x}_{1-AC} \\ \bar{x}_{2-AC} \\ \bar{x}_{3-AC} \end{bmatrix} = \begin{bmatrix} \bar{x}_{1-AC} \\ V_{AC} \\ 0 \end{bmatrix} \quad (18)$$

$$\bar{y}_{AC} = \begin{bmatrix} \bar{v}_{\alpha-AC} \\ \bar{v}_{\beta-DC-AC} \\ \bar{v}_{DC-AC} \end{bmatrix} = \begin{bmatrix} \bar{x}_{2-AC} \\ \omega \bar{x}_{1-AC} \\ 0 \end{bmatrix} = \begin{bmatrix} V_{max} \sin(\omega t + \varphi) \\ -V_{max} \cos(\omega t + \varphi) \\ 0 \end{bmatrix} \quad (19)$$

where  $V_{max}$  indicates the maximum input voltage and the constant state is indicated by ( $\bar{\cdot}$ ).

The following is an expression for the output vector ( $\hat{\omega} \neq \omega$ ):

$$\bar{y}_{AC} = \begin{bmatrix} \bar{v}_{\alpha-AC} \\ \bar{v}_{\beta-AC} \\ \bar{v}_{DC-AC} \end{bmatrix} = \begin{bmatrix} V_{\alpha-max} \sin(\omega t + \varphi - \phi) \\ -V_{\beta-max} \cos(\omega t + \varphi - \phi) \\ \frac{\omega}{\sqrt{\omega_f^2 + \omega^2}} (V_{AC} - \bar{v}_{\alpha-AC}) \end{bmatrix} \quad (20)$$

The values of  $V_{\alpha-max}$ ,  $V_{\beta-max}$ , and  $\phi$  are calculated. Equations [19] and [20] illustrate that the output vector steadily retains its sinusoidal waveforms even after the frequency estimation loop is turned off. Regarding the stability of the modified FLL, when the SOGI-FLL is subjected to an input voltage that takes a sinusoidal form at frequency  $\omega$  and there is a slight difference between the input frequency and the estimated frequency, as per [20], the relationship between states in a steady state can be approximated by [21] [20]:

$$\begin{cases} \dot{\bar{x}}_{2-AC} = -\omega^2 \bar{x}_{1-AC} \\ \bar{x}_{3-AC} = 0 \end{cases} \quad (21)$$

Thus, the steady-state frequency error can be expressed from [20] and [21] as follows:

$$\bar{\zeta}_f = (\hat{\omega} \bar{x}_1 - k \bar{x}_3)(\bar{v} - \bar{x}_2 - \bar{x}_3) = (\hat{\omega}(\bar{x}_{1-DC} + \bar{x}_{1-AC}) - k(\bar{x}_{3-DC} + \bar{x}_{3-AC}))(\bar{v}_{DC} - \bar{x}_{2-DC} - \bar{x}_{3-DC} + \bar{v}_{AC} - \bar{x}_{2-AC} - \bar{x}_{3-AC}) \quad (22)$$

In addition, from [19]-[21], [23] becomes:

$$\bar{\zeta}_f = (\hat{\omega} \bar{x}_1 - k \bar{x}_3)(\bar{v} - \bar{x}_2 - \bar{x}_3) = \hat{\omega} \bar{x}_{1-AC} (\bar{v}_{AC} - \bar{x}_{2-AC}) \quad (23)$$

Consequently, using equations [21]-[23], the following is a description of the frequency inaccuracy in the steady state:

$$\bar{\zeta}_f = \frac{\bar{x}_{1-AC}}{k} (\dot{\bar{x}}_{2-AC} + \hat{\omega}^2 \bar{x}_{1-AC}) = \frac{\bar{x}_{2-AC}^2}{k} (\hat{\omega}^2 - \omega^2) \quad (24)$$

This formulation shows that the  $\bar{\zeta}_f$  term collects data on the frequency estimation error, making it an appropriate control signal for the FLL block. By presuming, it is possible to analyze the FLL's local stability  $\hat{\omega} \approx \omega$ . Within this context, the term  $\hat{\omega}^2 - \omega^2$  can be approximated to  $2\omega(\hat{\omega} - \omega)$ , which allows describing the local dynamics of the FLL as follows:

$$\dot{\hat{\omega}} = -\gamma \bar{\zeta}_v = -\gamma \frac{2\hat{\omega}\bar{x}_2 - AC^2}{k} (\hat{\omega} - \omega) \quad (25)$$

The frequency estimate error is defined as  $\delta = (\hat{\omega} - \omega)$ , the derivative of  $\delta$  is given by  $\dot{\delta} = \dot{\hat{\omega}}$  [assuming  $\omega$  remains constant]. For positive values of  $\hat{\omega}$ , the assertion in [26] is thus valid; this condition is essential to the FLL's local stabilizing mechanism:

$$\dot{\delta} = -\gamma \frac{2\hat{\omega}\bar{x}_2 - AC^2}{k} \delta^2 \leq 0 \quad (26)$$

This approach ensures convergence, eliminating the DC component from the FLL estimator inputs in a steady state. Consequently, the DC offset estimation block does not affect the proposed FLL scheme's stability.

## 4. Experimental results

Experimental tests are carried out to validate the effectiveness of the proposed control approach. The setup used in this experiment is portrayed in Figure 4, with the parameters given in Table 2. Note that the components used in the hardware test based on the Micro-labBoxDspace of Figure 4 are as follows:

- speed sensor Incremental encoder DC /5V/24V /4096/ P/R,
- control desk and Ds1102 Micro LabBox,
- the torque control unit and powder brake,
- numerical oscilloscope,
- current sensor,
- three-phase inverter composed of IGBT and rectifier.

The proposed speed controller is evaluated under several load conditions, including both loaded and unloaded scenarios, with the ESOGI-FLL estimator. The obtained results in the non-load state of the motor, namely between 1000 r/min and 1300 r/min, for variations in reference speed, are shown in Figure 5. In Figure 5(a), the displayed data illustrates the measured speed responses alongside the estimated and referred values. The reference speed and estimated speed are seen to be closely aligned. Furthermore, a little delay is discernible when the speed reference changes modification. The motor's performance is unaffected by this delay, as shown in Figure 5(b). The proposed method for controlling the estimated speed can be assessed by comparing it to a reference system that exhibits excellent transient responsiveness. Figures 5(a) to (d) show the change in speed with a difference in the current phase amplitude measured, and the frequency is estimated via the ESOGI-FLL estimator. Most estimators that have been introduced are used to estimate the frequency. We cannot estimate the negative speed due to the absence of a negative frequency, which necessitated us to enhance the design of ESOGI-FLL. It is proposed that a speed reference component be incorporated. We change the reference from [1200 to -1200] inversion of direction, and at no load, Figure 6(a) shows that the estimated speed follows its reference perfectly. The

present phase [ja] and its amplitude exhibit variation when there is a change in the speed within their reference. The frequency and phase shown in Figure 6 are estimated to stay constant regardless of the fluctuating load, only exhibiting modifications in response to variations in speed.

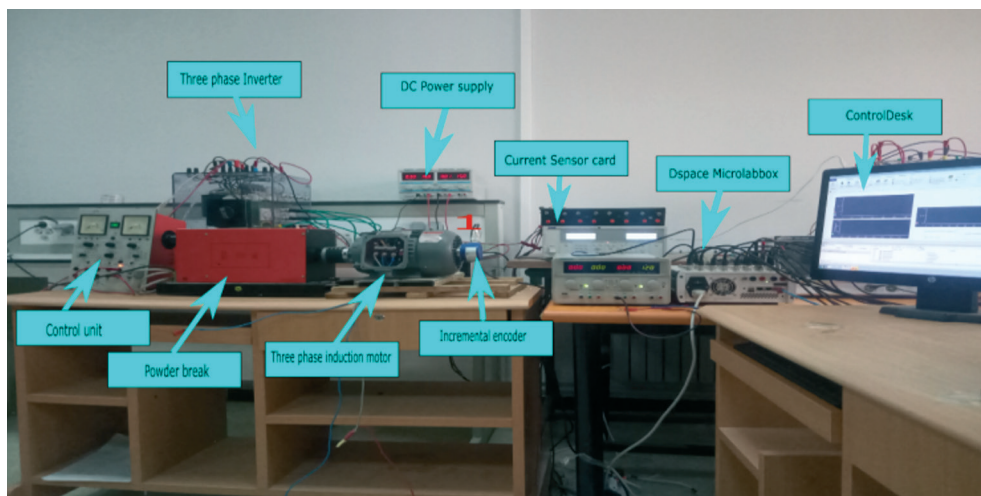
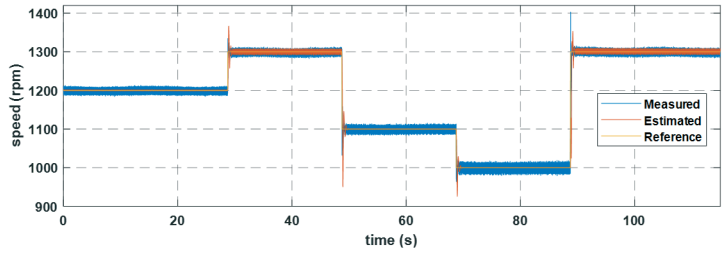


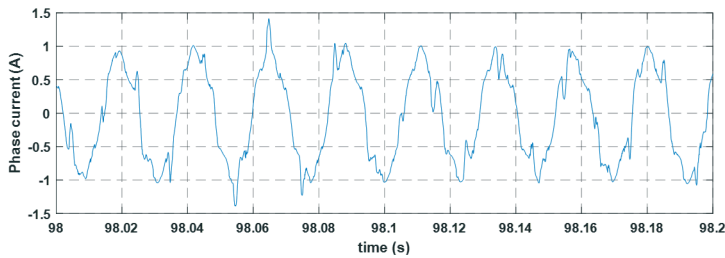
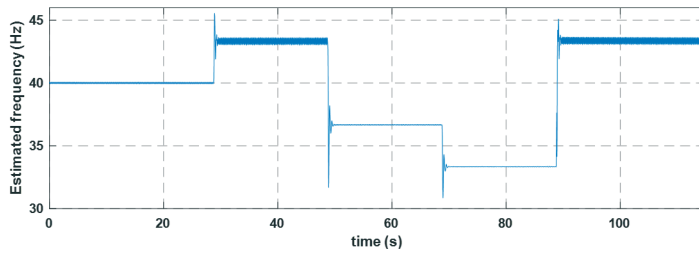
Fig. 4. Used Laboratory Equipment Kit

Tab. 2. System and Control Parameters

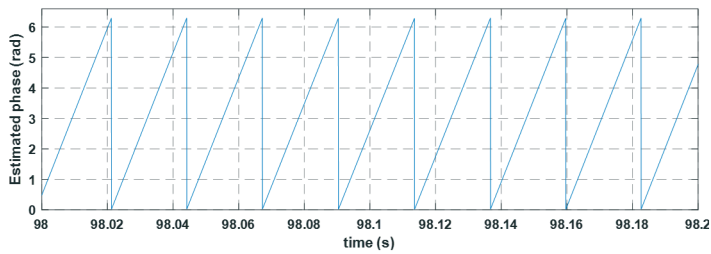
Parameter	Value
Nominal voltage ( $v$ )	220 V
Nominal Frequency ( $f$ )	50 Hz
DC Voltage ( $U_{dc}$ )	450 V
IM nominal speed ( $\omega_s$ )	1390 rpm
Number of pole pairs ( $p$ )	2
Proportional gain ( $k_p$ )	10
Integral gain ( $k_i$ )	0.001



(a) Reference speed and estimated

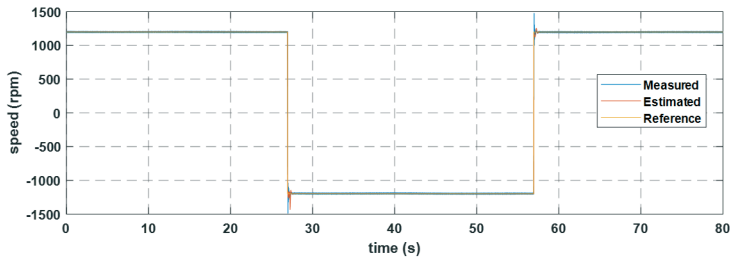
(b) Phase current ( $i_a$ )

(c) Estimated frequency

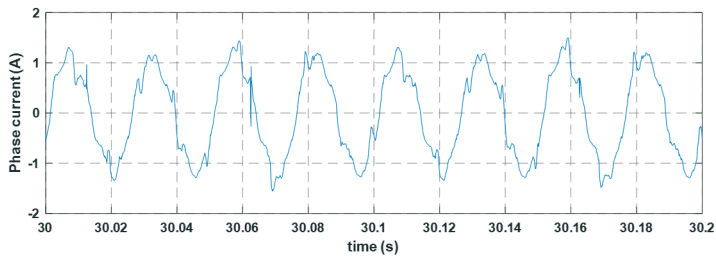


(d) Estimated phase

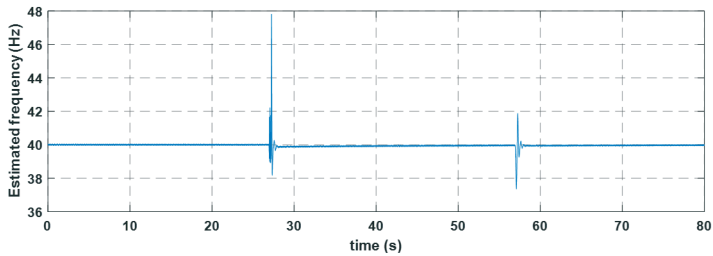
**Fig. 5. Proposed controller performance in experiments with reference variation**



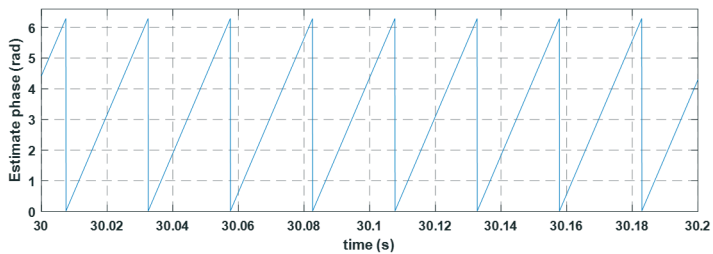
(a) Reference and estimated speed



(b) Current amplitude and zoom in current phase a



(c) Estimated frequency

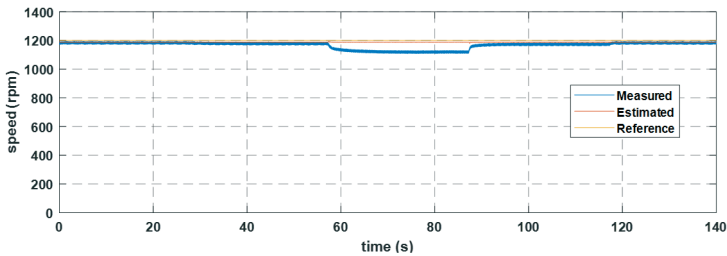


(d) Estimated phase

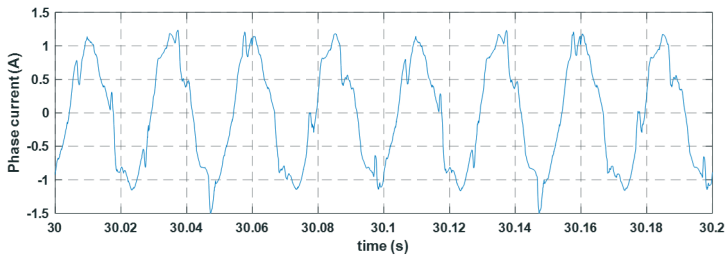
**Fig. 6. Performance of the proposed controller based on ESOGI-FLL estimator in experiments with speed inverse**

The latter is applied to varied speed profiles. From the above results, we can see that the performance is satisfactory. This improvement is seen in the speed signal quality level [smaller bandwidth according to Figure 7(a), as well as at the level of the almost total rejection of the disturbance [load torque] in the presence of a torque load [2 Nm] than that applied in the case of ESOGI-FLL estimator. The estimation is efficient and converges quickly towards a value close to the nominal value of the current amplitude changes with the applied load, as shown in Figure 8(b). The estimated frequency is immediately connected with the estimated speed as the latter remains unchanged with the applied load Figure 8(c).

Based on the motor test results, we can conclude that the proposed ESOGI-FLL-based control scheme effectively tracks rotor speed across a broad range of speeds and under different load conditions.

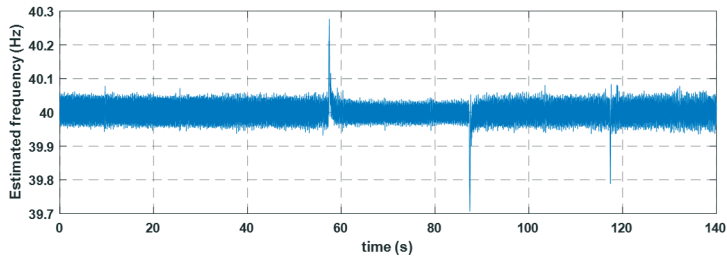


(a) Reference, measured speed, and estimated

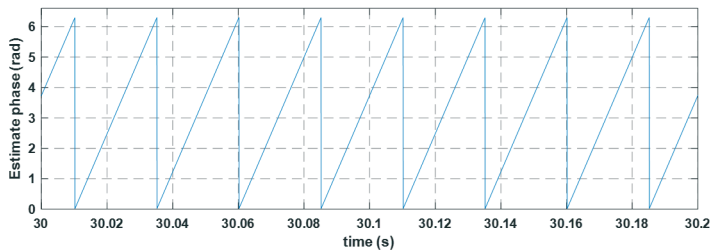


(b) Current amplitude and zoom in current phase a

**Fig. 7. Proposed control scheme performance in experiments with changing loads**



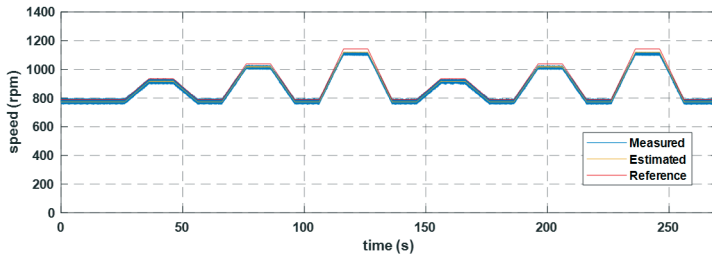
(c) Estimated frequency



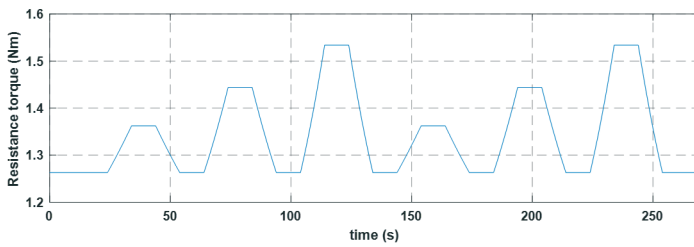
(d) Estimated phase

**Fig. 7. Proposed control scheme performance in experiments with changing loads; cont.**

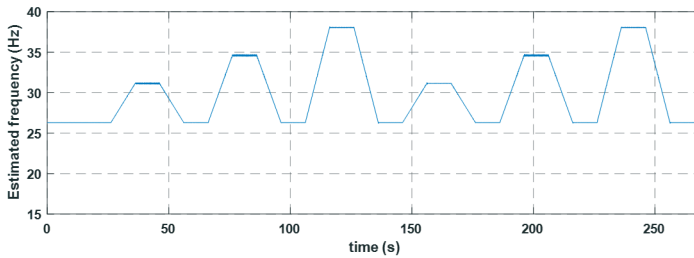
In the final test, a cyclic drive of the vehicle dynamic model is applied to the induction motor, as illustrated in Figure 8(a). The results demonstrate that the estimated and measured speeds closely match the reference speed, exhibiting good performance and accuracy, with only a slight static error at higher speeds. Additionally, the motor load, applied as a cycle, is depicted in Figure 8(b). Figures 8(c) and 8(d) present the corresponding estimated frequency and phase angle.



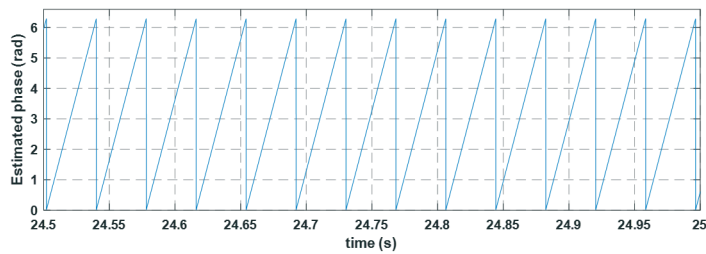
(a) Speed reference profiles and estimated speed



(b) Resistance torque ( $T_r$ )



(c) Estimated frequency



(d) Estimated phase

**Fig. 8. EV's Performance under speed cycle variation**

**Tab. 3. Comparison of ESOGI-FLL with other sensorless methods**

Observer/Estimator	Affected by parameter change	DC offset elimination	Realization cost
ESOGI-FLL	✗	✓	low
SOGI-FLL	✗	✗	low
MRAS	✓	✗	high
Luenberger	✓	✗	high
SMD	✓	✗	high
EKF	✓	✗	high

Table 3 compares ESOGI-FLL with other sensorless control methods, highlighting key features. It reveals that MRAS, Luenberger, SMD, and EKF methods each require at least four sensors, are sensitive to variations in motor parameters, lack DC offset elimination, and involve greater implementation complexity compared to SOGI-FLL and ESOGI-FLL. While SOGI-FLL and ESOGI-FLL exhibit similar performance, ESOGI-FLL demonstrates a clear advantage in effectively rejecting DC offset. Therefore, ESOGI-FLL emerges as the most suitable method for speed estimation.

## 5. Conclusion

A significant challenge with most speed-sensorless controllers is their inability to reject disturbances. This work proposed a sensorless control scheme based on ESOGI-FLL to address this issue and ensure appropriate regulation of an IM drive with enhanced performance under various disturbances. The ESOGI-FLL, designed for harmonics and DC offset rejection, was introduced as a speed estimator using only one single-phase sensed current of the IM. It demonstrated high estimation accuracy, particularly during frequency ramps and while compensating for DC disturbance. Moreover, employing a single current sensor makes the control system cost-effective and efficient. Experimental validation using the dSPACE MicroLab Box confirmed the robustness of the ESOGI-FLL-based controller, ensuring high-performance speed tracking under IM speed variations, even under distorted currents inherent DC disturbance.

## 6. References

- [1] Freitas JBS, Marquezan L, de Oliveira Evald PJD, Peñaloza EAG, Cely MMH. A fuzzy-based predictive PID for DC motor speed control. *International Journal of Dynamics and Control*. 2024;12(7):2511-2521. <https://doi.org/10.1007/s40435-023-01368-2>.
- [2] Özçiflikçi OE, Koç M, Bahçeci S, Emiroğlu S. Overview of PMSM control strategies in electric vehicles: a review. *International Journal of Dynamics and Control*. 2024;12(6):2093-2107. <https://doi.org/10.1007/s40435-023-01314-2>.

- [3] Kumar V, Chenchireddy K, Sreejyothi KR, Sujatha G. Design and Development of Brushless DC Motor Drive for Electrical Vehicle Application. AI Enabled IoT for Electrification and Connected Transportation. Singapore. Springer Nature Singapore. 2022:201–217. [https://doi.org/10.1007/978-981-19-2184-1\\_10](https://doi.org/10.1007/978-981-19-2184-1_10).
- [4] Van Meer M, González RA, Witvoet G, Domen T. Nonlinear bayesian identification for motor commutation: Applied to switched reluctance motors. 62nd IEEE Conference on Decision and Control (CDC). 2023:5494–5499. <https://doi.org/10.1109/CDC49753.2023.10384122>.
- [5] Chen J, Huang J. Stable simultaneous stator and rotor resistances identification for speed sensorless IM drives: Review and new results. IEEE Transactions on Power Electronics. 2017;33(10):8695–8709. <https://doi.org/10.1109/TPEL.2017.2785330>.
- [6] Xu D, Wang B, Zhang G, Wang G, Yu Y. A review of sensorless control methods for AC motor drives. CES Transactions on electrical machines and systems. 2018;2(1):104–115. <https://doi.org/10.23919/TEMS.2018.8326456>.
- [7] Nurettin A, İnanç N. Sensorless vector control for induction motor drive at very low and zero speeds based on an adaptive-gain super-twisting sliding mode observer. IEEE Journal of Emerging and Selected Topics in Power Electronics. 2023;1(4):4332–4339. <https://doi.org/10.1109/JESTPE.2023.3265352>.
- [8] Kanakabettu AKM, Irvathoor RB, Saralaya S, Jodumutt SB, Singh AB. Novel Advanced Artificial Neural Network-Based Online Stator and Rotor Resistance Estimator for Vector-Controlled Speed Sensorless Induction Motor Drives. Energies. 2024;17(9):2150. <https://doi.org/10.3390/en17092150>.
- [9] Zerdali E, Barut M. The comparisons of optimized extended Kalman filters for speed-sensorless control of induction motors. IEEE Transactions on industrial electronics. 2017;64(6):4340–4351. <https://doi.org/10.1109/TIE.2017.2674579>.
- [10] Jayaramu ML, Suresh HN, Bhaskar MS, Almakhlles D, Padmanaban S, Subramaniam U. Real-time implementation of extended kalman filter observer with improved speed estimation for sensorless control. IEEE Access. 2021;9:50452–50465. <https://doi.org/10.1109/ACCESS.2021.3069676>.
- [11] Wang H, Yang Y, Ge X, Zuo Y, Yue Y, Li S. PLL-and FLL-based speed estimation schemes for speed-sensorless control of induction motor drives: Review and new attempts. IEEE Transactions on Power Electronics. 2021;37(3):3334–3356. <https://doi.org/10.1109/TPEL.2021.3117697>.
- [12] Nguyen ND, Nam NN, Yoon C, Lee YI. Speed sensorless model predictive torque control of induction motors using a modified adaptive full-order observer. IEEE Transactions on Industrial Electronics. 2022;69(6):6162–6172. <https://doi.org/10.1109/TIE.2021.3094493>.
- [13] Xin Z, Zhao R, Blaabjerg F, Zhang L, Loh PC. An improved flux observer for field-oriented control of induction motors based on dual second-order generalized integrator frequency-locked loop. IEEE Journal of Emerging and Selected Topics in Power Electronics. 2016;5(1):513–525. <https://doi.org/10.1109/JESTPE.2016.2623668>.
- [14] Zhao R, Xin Z, Loh PC, Blaabjerg F. A novel flux estimator based on multiple second-order generalized integrators and frequency-locked loop for induction motor drives. IEEE Transactions on Power Electronics. 2017;32(8):6286–6296. <https://doi.org/10.1109/TPEL.2016.2620428>.
- [15] Wang H, Yang Y, Zuo Y, Li S, Hu X, Ge X. A speed estimation scheme based on an improved SOGI-FLL for speed-sensorless control of induction motor drives. Proceedings – IECON 2020: 46th Annual Conference of the IEEE Industrial Electronics Society. 2020:852–857. <https://doi.org/10.1109/IECON43393.2020.9255253>.
- [16] Bouzidi R, Ghadbane I, Boukhari M, Bendib A, Kherbachi A. Experimental implementation of low-cost and robust sensorless control based on SOGI-FLL estimator for electric vehicles. International Journal of Power Electronics and Drive Systems. 2022;13(4):1993–2004. <https://doi.org/10.11591/ijpeds.v13.i4.pp1993-2004>.
- [17] Lee K, Han Y. Reactive-power-based robust MTPA control for v/f scalar-controlled induction motor drives. IEEE Transactions on Industrial Electronics. 2022;69(1):169–178. <https://doi.org/10.1109/TIE.2021.3055183>.

- [18] Bendib A, Chouder A, Kara K, Kherbachi A, Barkat S, Issa W. New modeling approach of secondary control layer for autonomous single-phase microgrids. *Journal of the Franklin Institute*. 2019;356(13):6842–6874. <https://doi.org/10.1016/j.jfranklin.2019.04.020>.
- [19] Golestan S, Guerrero JM, Vasquez JC, Abusorrah AM, Al-Turki Y. Modeling, tuning, and performance comparison of second-order-generalized-integrator-based FLLs. *IEEE Transactions on Power Electronics*. 2018;33(12):10229–10239. <https://doi.org/10.1109/TPEL.2018.2808246>.
- [20] Kherbachi A, Chouder A, Bendib A, Kara K, Barkat S. Enhanced structure of second-order generalized integrator frequency-locked loop suitable for DC-offset rejection in single-phase systems. *Electric Power Systems Research*. 2019;170:348–357. <https://doi.org/10.1016/j.epsr.2019.01.029>.

## Appendix 1

- $\hat{\omega}$  : the estimated frequency
- $\omega_f$  : LPF cut-off frequency
- $k$  : stands for a positive adjustable gain
- $\gamma$  : a positive constant
- $x$  : the state vector
- $y$  : the output vector
- $v_{DC/AC}$  : the input voltage and AC components
- $x_{DC/AC}$  : the state vector DC and AC components
- $y_{DC/AC}$  : the output vector DC and AC components
- $V_{DC}$  : the DC-offset component of the input voltage
- $V_{max}$  : the magnitude of the input voltage
- $(\bar{\phantom{x}})$  : stands for the steady-state condition
- $V_{\alpha-max}$  : the magnitudes of the output voltage  $V_{\alpha}$
- $V_{\beta-max}$  : the magnitudes of the output voltage  $V_{\beta}$
- $\phi$  : the phase angle between the input and the in-phase component
- $\zeta_f$  : the frequency error
- $\zeta^f$  : the frequency error
- $\zeta_v$  : the voltage error
- $\delta$  : the error in frequency estimation